ChemElectroChem

Research Article
doi.org/10.1002/celc.202101559

Chemistry Europe
European Chemical Societies Publishing

www.chemelectrochem.org

Special Collection

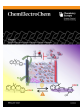

Electrocarboxylation of Spiropyran Switches through Carbon-Bromide Bond Cleavage Reaction

Sara Santiago, Clara Richart, Silvia Mena, Iluminada Gallardo, Jordi Hernando,* and Gonzalo Guirado*[a]

This manuscript deals with carbon capture and utilization to synthetize high-added chemicals using CO_2 as a C1-organic building block for C–C bond formation. The study focuses on the electrocarboxylation of 1,3,3-trimethylindolino-6′-bromo-benzopyrylospiran switch (**Br-BIPS**). Prior to the electrocarboxylation process, the electrochemical reduction mechanism of **Br-BIPS** and CO_2 is disclosed in polar aprotic solvents using two different cathodes (glassy carbon and silver) under nitrogen atmosphere. Once the role of the cathode in the reduction carbon-bromide bond cleavage is understood, carboxylated spiropyran derivatives can be synthesized in moderate yields and conversion rates through an electrocarboxylation process using CO_2 silver cathode and polar aprotic solvents. The "green" efficient route described in the current work would open a new sustainable strategy for designing and building "smart" surfaces with switchable physical properties.

Introduction

Photoswitches are a class of molecules or organometallic complexes that undergo a reversible interconversion between different states triggered by light.[1] Spiropyrans are amongst the most studied of these systems, which toggle between spirocyclic (**SP**) and merocyanine (**MC**) isomers upon light-induced ring-opening and ring-closing reactions, respectively (Figure 1).[2–5] These two states show markedly distinctive geometrical and physicochemical properties, such as different effective pKa values,[6–9] dipole moments (from ~4–6 D (**SP**) to ~18 D (**MC**))[10] or emission properties.[11] However, the most remarkable change observed upon spiropyran photoisomerization is the difference in UV-vis absorbance: while **SP** is transparent in the visible range, **MC** shows a very intense absorption peak in that region. This means that light-induced **SP**-**MC** interconversion is accompanied by an intense variation in coloration, a phenomenon known as photochromism.[12,13]

Because of the large change in properties upon photoisomerization, spiropyrans have been exploited for the preparation of a wide variety of smart functional materials whose properties can be very precisely controlled using light as an external stimulus.[14–18]

For most of these applications, the photoswitchable molecules must be covalently attached to the final materials, such as polymers,[19–21] nanoparticles,[22,23] biomacromolecules[24,25] and surfaces,[26,27] which requires the introduction of suitable groups in spiropyrans to ensure chemical functionalization. Carboxylic acid groups are amongst the most preferred for this purpose, as they confer molecules with a broad reactivity that enables the covalent bonding to substrates by simple coupling reactions (e.g., amide bond formation).[26,28,29] However, the incorporation of carboxylic acids in spiropyrans is not straightforward, typically involves several synthetic steps (e.g., condensation of an aromatic aldehyde with enamine indole) and moderate yields.[30–32]

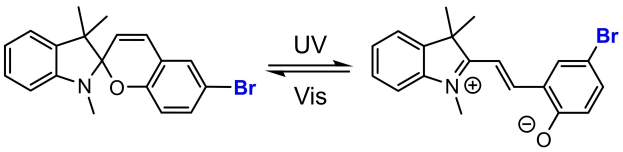

Figure 1. Photoisomerization of spiropyrans between the closed SP form and the open MC structure.

Actually, the chemical synthesis of carboxylic acids and their derivatives (e.g., esters or amides) imply the use of many reagents, catalysts[33] or organolithium compounds[34] at mild or strong conditions.[35,36] In this context, the electrochemical carboxylation of organic molecules to produce carboxylic acids by fixing carbon dioxide has emerged during the last years as an efficient *green* route compared to conventional chemical synthetic methods, especially since this process can be performed efficiently under mild conditions at atmospheric pressure and avoiding the use of additional reagents.[37–42] One of the most popular electrocarboxylation strategies of organic compounds is based on the *in situ* formation of a carbanion via reduction, which in turn undergoes a nucleophilic addition to CO_2 to yield the carboxylate functional group (Figure 2).[43] The success of this approach is strongly related to the stability (i.e., lifetime) of the anion formed in the electrolytic medium. In

[a] S. Santiago, C. Richart, Dr. S. Mena, Prof. I. Gallardo, Dr. J. Hernando, Dr. G. Guirado
Departament de Química
Universitat Autònoma de Barcelona
Bellaterra (Barcelona), 08193, Spain
E-mail: Jordi.Hernando@uab.cat
Gonzalo.Guirado@uab.cat

Supporting information for this article is available on the WWW under https://doi.org/10.1002/celc.202101559

Special Collection *An invited contribution to a Special Collection on Current Trends in Electrochemistry 2021 for the 1st French-Spanish Workshop on Electrochemistry.*

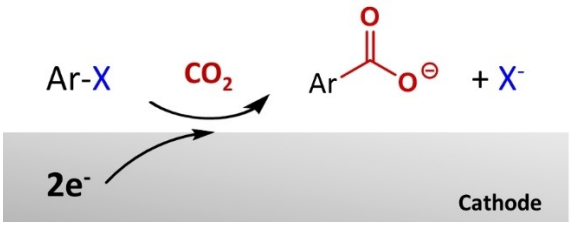

Figure 2. Representation of the electrochemical carboxylation of aryl halides using CO_2.

order to increase its lifetime, it is highly desirable to decrease the reduction potential at which the carbanion is produced. This goal can be achieved by the use of aryl halides, which can be electrochemically reduced leading to the desired anionic species after C–X bond cleavage at relatively low potentials in organic aprotic solvents.[44]

Given the advantages of electrocarboxylation processes and their reported success on simple, model aryl halides such as bromobenzene,[43] herein we attempted the carboxylation reaction of much more challenging spiropyran substrates by electrochemical reduction of a commercially available bromo-spiropyran derivative under CO_2 atmosphere. In addition, the effect of the nature of the cathode (carbon and silver) was evaluated in terms of performance and energy efficiency, since it is well known the electrocatalytic effect of using silver in the reduction of organic halides.[45–48] Our work therefore showcases a new one-pot and facile strategy for the functionalization of the spiropyran backbone using CO_2 (as a C1-buidling block) and electrochemical techniques. Such an attractive and environmentally friendly approach could grant access to a broad variety of carboxylated spiropyran derivatives, which could be eventually applied for the design of smart surfaces and devices.

Experimental Section

Reagents

1,3,3-trimethylindolino-6′-bromobenzopyrylospiropyran (**Br-BIPS**, pur. 98.0%) was purchased from TCI Chemicals and used without further purification. High purity CO_2 and Ar gases (IC 5.0) used for the electrochemical measurements and electrosynthesis were supplied by Linde.

Anhydrous and extra pure tetrabutylammonium hexafluorophosphate, ($TBAPF_6$; pur. >99.0%), iodomethane (MeI; pur. >99.0%) and anhydrous sodium sulfate (Na_2SO_4; pur. >99.0%) were acquired from Merck. Anhydrous *N,N*-dimethylformamide (DMF; pur. >99.5%) and anhydrous dimethylsulfoxide (DMSO; pur. >99.8%) were purchased from Acros Organics. Both solvents were dried under activated molecular sieves of 4 Å prior to use to ensure water content <100 ppm for the electrochemical measurements and electrosynthesis.

Dichloromehtane (DCM, pur. >98%), *n*-hexane (pur. >98%) and ethyl acetate (pur. >98%) used for the purification of the products prepared by electrosynthesis were obtained from SDS and used as received.

Instrumentation and procedure

Electrochemical studies were performed by cyclic voltammetry (CV) using the potentiostat Workstation CHInstrument and controlled by the software CHI660e V14.08. For these measurements, a three-electrode system and a thermostatic electrochemical cell was used. Glassy carbon (WE_C, 1 mm of diameter) or silver (WE_{Ag}, 3 mm of diameter) were used as working electrodes, while a platinum wire and a saturated calomel electrode (SCE) were used as counter (CE, and reference (Ref) electrodes, respectively. Both CE and Ref electrodes were separated from the solution by a salt-bridge. Solutions at different concentration of **Br-BIPS** (in the range of 3–10 mM) were prepared in DMF/0.1 M of $TBAPF_6$. Prior to each measurement, the solutions were purged with either Ar or CO_2 depending on the type of study in each case. In the case of CO_2 gas, the flow was controlled using a Mass Flow Meter.

The Bulk Electrolysis were carried out at controlled constant potential using the potentiostat EG&G Princeton Applied Research model 273 A. For these experiments, we used the same electrochemical setup as for CV measurements but replacing the small diameter sized WE_C or WE_{Ag} for a large area graphite rod (area: ~8 cm^2) or silver foil (area: ~6 cm^2), respectively. For the electrolysis of **Br-BIPS** under inert atmosphere, the solution was purged with Ar for 10 min and then the corresponding reduction potential was applied until a total charge of 2 F was passed (−2.35 V when using WE_C and −2.00 V for WE_{Ag} vs SCE). For the purification of the products after the electrolysis, firstly the solvent of the reaction mixture was removed under vacuum and then an extraction in diethyl ether: H_2O (2:1) was performed. Then, the organic phase was washed for three times with water (2:1 v/v ratio), dried with anhydrous Na_2SO_4 and the solvent evaporated in vacuo.

Analogously, for the electrolysis under CO_2 atmosphere, the solution was saturated in this gas by bubbling for 20 minutes. After that, a constant reduction potential was applied until 2 F of total charge were reached (−2.35 V when using WE_c and −2.00 V for WE_{Ag} vs SCE). Immediately after, 10 equivalents of MeI were added to the solution to derivatize the carboxylate goup introduced and facilitate the isolation of the resulting methylated product **BIPS-COOMe**. The solvent of the reaction mixture was removed under vacuum and purified performing a preparative thin layer chromatography (TLC). A mixture of *n*-hexane and ethyl acetate (80:20 v/v ratio) was used as a mobile phase.

The products **BIPS** and **BIPS-COOMe** obtained after the electrosynthesis of the reagent **Br-BIPS** under Ar and CO2 atmosphere, respectively, were characterized by attenuated total reflectance infrared spectroscopy (ATR-FTIR), H ^{1}NMR on a Brucker spectrometer DPX360 and electrospray mass spectrometry (ESI-MS).

Br-BIPS: ^{1}H NMR (360 MHz, Chloroform-*d*) δ 1.16 (s, 3H), 1.29 (s, 3H), 2.71 (d, J=1.6 Hz, 3H), 5.72 (d, J=10.3 Hz, 1H), 6.53 (d, J=7.7 Hz, 1H), 6.60 (d, J=9.3 Hz, 1H), 6.78 (d, J=10.2 Hz, 1H), 6.85 (td, J=7.4, 1.0 Hz, 1H), 7.07 (dd, J=7.3, 1.3 Hz, 1H), 7.16 (ddt, J=5.4, 3.9, 1.8 Hz, 3H). ESI-MS: m/z found for $C_{19}H_{18}BrNO$ (M+H): 358.0781 (100%); 359.0809 (24.4%); 360.0773 (97.2%); 361.0796 (19.9%).

BIPS ^{1}H NMR (360 MHz, $CDCl_3$) δ 1.18 (s, 3H), 1.32 (s, 3H), 2.74 (s, 3H), 5.68 (d, J=10.2 Hz, 1H), 6.54 (d, J=7.7 Hz, 1H), 6.72 (d, J=8.1 Hz, 1H), 6.78–6.89 (m, 3H), 7.01–7.14 (m, 3H), 7.19 (td, J=7.6, 1.3 Hz, 1H). ESI-MS: m/z found for $C_{19}H_{19}NO$ (M+H): 278.1539 (100%); 279.1572 (21.1%); 280.1604 (2.3%).

BIPS-COOMe: ^{1}H NMR (360 MHz, $CDCl_3$) δ 1.19 (s, 3H), 1.33 (s, 3H), 2.74 (s, 3H), 3.90 (s, 3H), 5.77 (d, J=10.1 Hz, 1H), 6.55 (d, J=7.6 Hz, 1H), 6.73 (d, J=7.6 Hz, 1H), 6.82–6.91 (m, 2H), 7.10 (d, J=7.2 Hz, 1H), 7.17–7.23 (m, 2H), 7.8 (s, 1H). ESI-MS: m/z found for $C_{21}H_{21}NO_3$ (M+H): 336.1581 (100%); 337.1616 (23.2%); 338.1701 (7.7%).

Results and Discussion

Electrochemical reduction of Br-BIPS in DMF

Electrochemical study under inert atmosphere (Ar)

The electrochemical behavior of the compound **Br-BIPS** was studied by CV at different concentrations (1–5 mM) and scan rates (0.1–1.0 V/s) under inert conditions (Ar) using *N,N*-dimethylformamide (DMF) as a solvent and 0.1 M of $TBAPF_6$ as a supporting electrolyte. As an example, Figure 3a shows the electrochemical response of a 5 mM solution of **Br-BIPS** recorded at 0.1 V/s scan rate and using two different working cathodes: glassy carbon (WE_C) and silver (WE_{Ag}). Figure 3b shows the cyclic voltammogram in a first cathodic scan, from −1.60 V to −2.70 V vs SCE, for a 5 mM solution of **Br-BIPS** using WE_C. Two irreversible peaks were found at $E_{pc} = -2.23$ V and −2.47 V (vs SCE), which could be attributed to two- and one-electron reduction processes, respectively (Figure 3b). It is worth noting that, when W_{Ag} was used as a working electrode instead, the two-electron irreversible reduction peak of **Br-BIPS** was registered at $E_{pc} = -1.92$ V (vs SCE) (Figure 3a). This potential shift of *ca.* 280 mV to less negative values indicates the electrocatalytic effect of the use of silver as a cathode (Figure 3a).

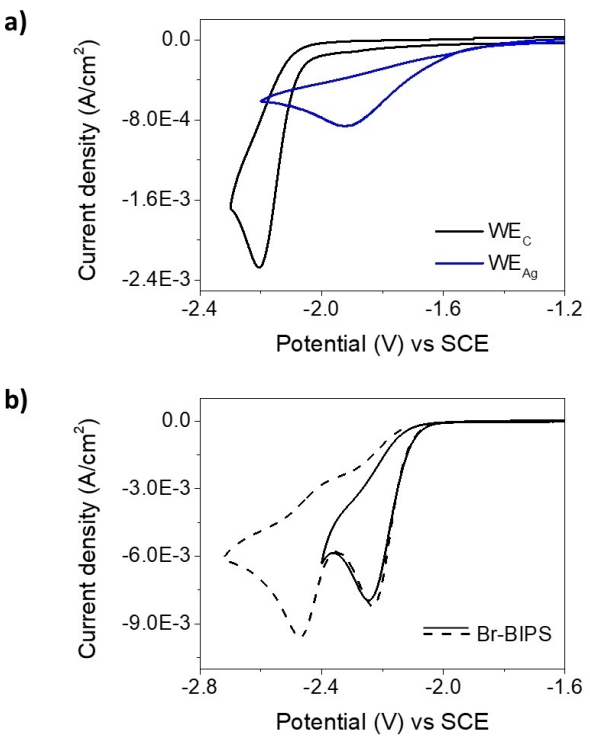

Figure 3. (a) CVs registered for a 5 mM solution of Br-BIPS in DMF/0.1 M $TBAPF_6$ under Ar atmosphere and using either glassy carbon or silver as working electrodes (scan rate = 0.1 V/s). (b) CVs registered for a 5 mM solution of Br-BIPS in DMF/0.1 M $TBAPF_6$ under Ar atmosphere and using glassy carbon as a WE (scan rate = 0.1 V/s). Two different independent measurements are shown, which differ in the minimum potential of the scan. In both cases, a two-electron irreversible wave at $E_{pc} = -2.23$ V was observed.

Irrespective of the working electrode used, the irreversibility of the two-electron reduction wave measured for **Br-BIPS** in DMF under Ar atmosphere indicates that there is an irreversible chemical reaction coupled to the electron transfer to this compound. To determine the nature of this chemical reaction, the dependence of E_{pc} with the scan rate (v) and concentration were examined by CV. From the plot of E_{pc} vs log v, a linear relationship was found with a slope value of 35 mV, whereas no variation of the cathodic peak potential was observed with the **Br-BIPS** concentration in solution (Figure S1). Hence, it is possible to conclude that the chemical reaction coupled to the first reduction process is a first order reaction.

In order to disclose the nature of the product irreversibly formed after the electrochemical reduction of **Br-BIPS**, electrolytic processes at a controlled constant potential (vs SCE) of −2.35 V (for a carbon graphite rod electrode) or −2.00 V (for a silver foil electrode) were conducted in DMF and under inert atmosphere. These electrolysis experiments were simultaneously monitored by CV with WE_C, where we observed that the reduction peak at $E_{pc} = -2.23$ V (vs SCE) associated to the reduction of **Br-BIPS** gradually decreased, and a new oxidation peak at $E_{pa} \sim +0.70$ V (vs SCE) concomitantly increased with the injection of charge (Figure S2). After the passage of 2 F, the electrolytic mixture was treated and the irreversible product formed was isolated and analyzed by ^{1}H NMR, ESI-MS, ATR-FITR and UV-vis spectroscopy. This allowed us to assign this product to the debrominated compound **BIPS**, which was obtained in a 56% yield when using the carbon graphite rod as a WE and a 91% yield for WE_{Ag}. The remaining 30% and 9% respectively correspond to unreacted starting material. Interestingly, this assignment was consistent with two significant features observed in our CV measurements. On the one hand, the anodic peak emerging during the electrolysis experiments at $E_{pa} \sim +0.70$ V (vs SCE) for WE_C could be attributed to the bromide anion produced during the debromination of **Br-BIPS** (Figure S2).[49] On the other hand, the second one-electron reduction wave registered for **Br-BIPS** at $E_{pc} = -2.47$ V (vs SCE) with WE_C matches the cathodic peak measured for a solution of pure **BIPS** in DMF under Ar atmosphere ($E_{pc} = -2.50$ V (vs SCE) using WE_C, Figure S3) Therefore, the latter further supports the formation of **BIPS** after the two-electron reduction process of **Br-BIPS**.

From all this data, we conclude that the electrochemical reduction of **Br-BIPS** proceeds through an ECE mechanism (Scheme 1). First, an electron transfer (E) takes place where the corresponding radical anion is formed (**[Br-BIPS]$^{-\bullet}$**). Then, a first order chemical reaction (C) leads to the cleavage of the C–Br bond of the compound, thus producing the radical intermediate species **[BIPS]$^{\bullet}$**. Subsequently, this radical species is reduced again by a second electron transfer (E) yielding an anionic form (**[BIPS]$^-$**). This second reduction step must present a less negative potential than the first electron transfer ($E^o_2 > E^o_1$), which would explain why a single cathodic wave associated to a two-electron reduction process was observed by CV. Finally, the anionic form **[BIPS]$^-$** is protonated by subtracting a proton from the solvent or the tetrabutylammonium ion of the supporting electrolyte, yielding the final product **BIPS**.

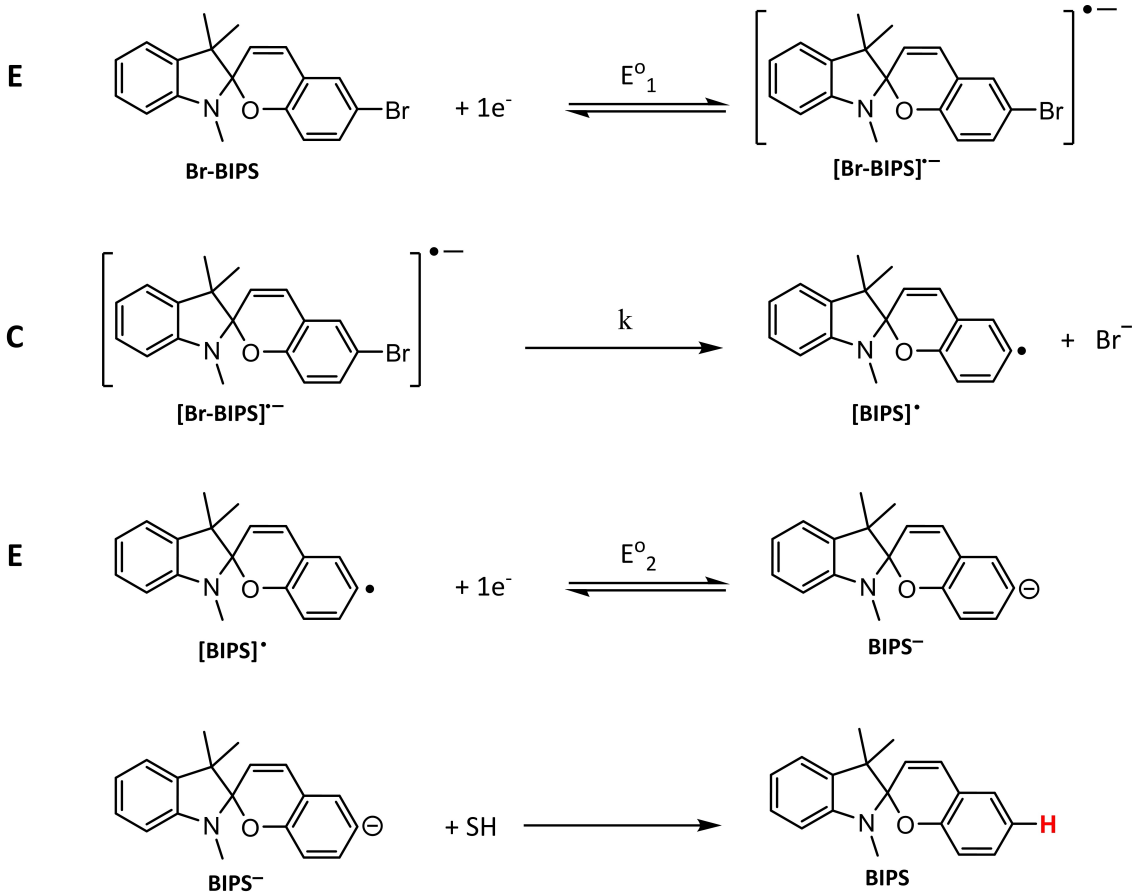

Scheme 1. Electrochemical reduction mechanism for Br-BIPS under inert atmosphere in DMF/0.1 M $TBAPF_6$. (SH is the solvent or the supporting electrolyte).

Electrochemical study under saturated atmosphere of CO_2

As the reduction of **Br-BIPS** leads to the formation of the carbanionic intermediate **BIPS**$^-$, we envisaged that this species could react with CO_2 to produce the target electrocarboxylated spiropyran derivative. To validate this hypothesis, we first investigated by CV the electrochemical properties of **Br-BIPS** in a 75 mM CO_2 DMF solution (Figure 4). Mainly, the same behavior previously observed under inert atmosphere was registered, and a two-electron irreversible reduction peak at $E_{pc} = -2.23$ V (vs SCE) or -1.92 V (vs SCE) was detected for WE_C or WE_{Ag}, respectively. Therefore, the electrocatalytic effect of the silver electrode was again demonstrated. When using WE_{Ag}, an additional irreversible cathodic wave at $E_{pc} = -2.60$ V (vs SCE) was measured, which can be attributed to the electrochemical reduction of the CO_2 present in solution.[26,49]

This was further proven by analyzing a pure DMF sample saturated with CO_2 by CV, where the same reduction peak at $E_{pc} = -2.60$ V (vs SCE) also appeared. In view of these results, it is possible to conclude that, in the presence of CO_2, the reduction of **Br-BIPS** follows the same ECE mechanism previously established under inert atmosphere, where the anionic intermediate **BIPS**$^-$ is electrogenerated.

Noticeably, when recording the full voltammogram of **Br-BIPS** under CO_2 atmosphere after the first cathodic scan (i.e., after irreversible producing **BIPS**$^-$), two different oxidation waves were observed in the anodic region (Figure 5). One of them appeared at $E_{pa} \sim +0.70$ V (vs SCE) for WE_C, which as previously mentioned, can be assigned to bromide anions and, therefore, is compatible with the reductive debromination of

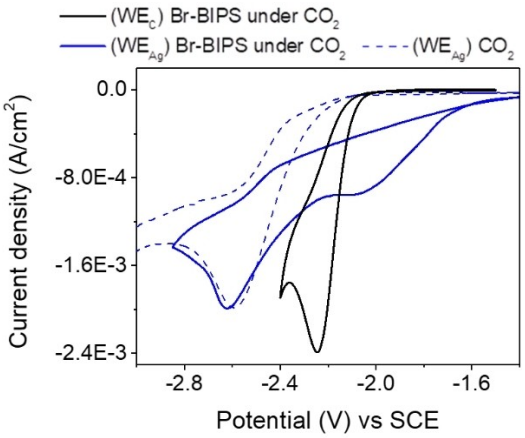

Figure 4. CVs (scan rate = 0.1 V/s) of a 5 mM solution of Br-BIPS in DMF/0.1 M $TBAPF_6$ under the presence of CO_2 using either glassy carbon (black solid line) or silver as a WE (blue solid line). For the case of WE_{Ag}, the electrochemical response of CO_2 in a neat DMF/0.1 M $TBAPF_6$ solution is also given (blue dashed line).

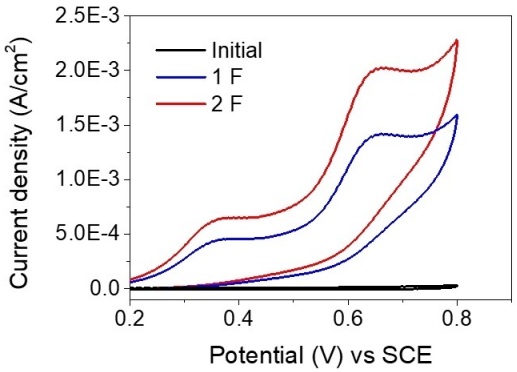

Figure 5. Cyclic voltammograms recorded to monitor the electrochemical reaction of Br-BIPS performed at a controlled constant potential in a partially saturated solution in CO_2 using glassy carbon as a WE. The CVs were recorded at 0.30 V/s in DMF/0.1 M of $TBAPF_6$ from 0.20 V to 0.80 V.

Br-BIPS. As for the second of the anodic peaks, it was registered at $E_{pa} \sim +0.40$ V (vs SCE) for WE_C and, more importantly, was not observed neither in the case of the electrochemical measurements of **Br-BIPS** nor the electrosynthesis of **BIPS** under inert atmosphere.

Consequently, this suggests that a different product is obtained when conducting the electrochemical reduction of **Br-BIPS** in the presence of CO_2, which must give rise to such an additional oxidation wave. We tentatively attributed this new peak to the oxidation of the carboxylate anion (**BIPS-COO$^-$**) obtained through the nucleophilic attack of the electrogenerated anionic form **BIPS$^-$** to the CO_2 molecules present in solution (Scheme 2). The low oxidation potential value obtained for the carboxylate **BIPS-COO$^-$** derivative is due to the aromatic electron rich system of the indole moiety. Similar anodic peak potential values were observed for other aromatic electron rich heterocycles, such as thiophenecarboxylate derivatives.[50]

To confirm the nature of the product obtained, bulk electrolysis of **Br-BIPS** in DMF and under CO_2 atmosphere were performed applying −2.35 V (vs SCE) or −2.00 V (vs SCE) for graphite rod or silver foil cathodes, respectively. The electrosynthesis was stopped after the passage of 2F (ca. 20 minutes) to avoid the obtention of non-desired overreduced compounds despite the fact that the reactant was not fully consumed, as further discussed below. To facilitate the isolation and identification of the electrocarboxylation product, 10 equivalents of CH_3-I were added to the solution after the electrosynthesis to further derivatize **BIPS-COO$^-$** and obtain the methyl ester **BIPS-COOMe**. The resulting samples were treated and the products generated were purified and analyzed by ^{1}H NMR, ESI-MS, ATR-FTIR and UV-vis absorption spectroscopy. As shown in Figure 6 three main compounds were identified in this way: (i) the unreacted starting material **Br-BIPS**, which was recovered; (ii) the byproduct **BIPS** in *ca.* 30% yield for both electrodes, which should arise from the competing protonation reaction of **BIPS$^-$** with the solvent or the supporting electrolyte; (iii) the desired carboxylated product **BIPS-COOMe**, which was obtained in 16% or 35% yield when either carbon or silver cathodes were

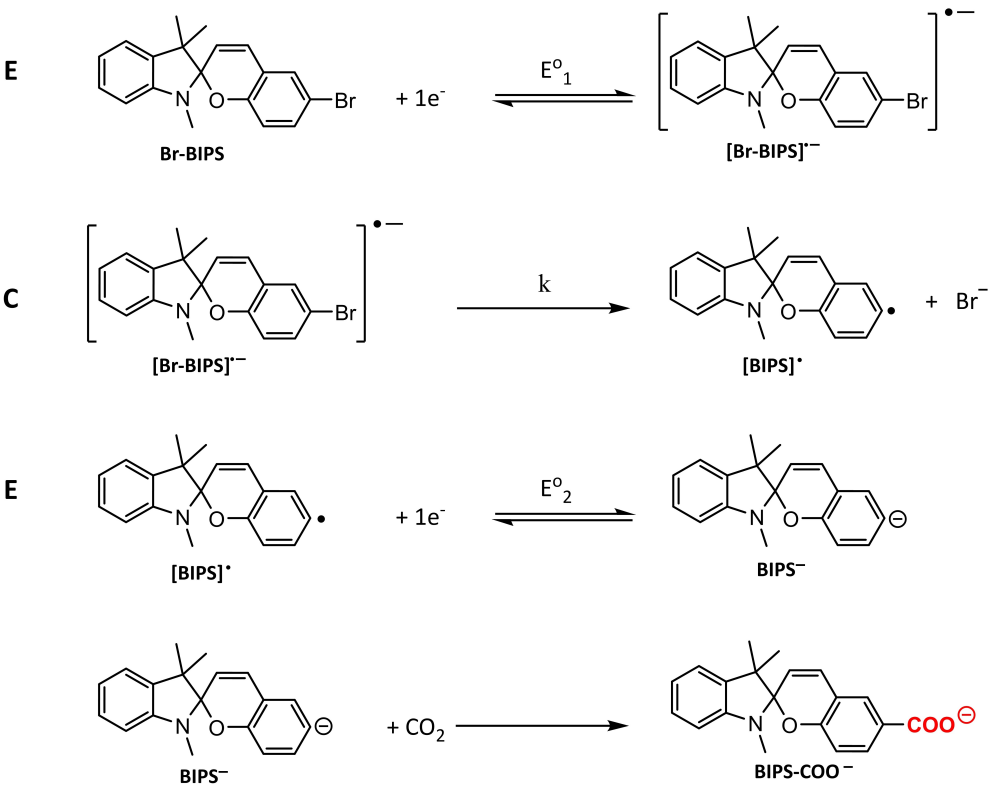

Scheme 2. Electrochemical reduction mechanism for Br-BIPS in DMF/0.1 M $TBAPF_6$ saturated with CO_2, which eventually leads to the formation of the electrocarboxylated product BIPS-COO$^-$.

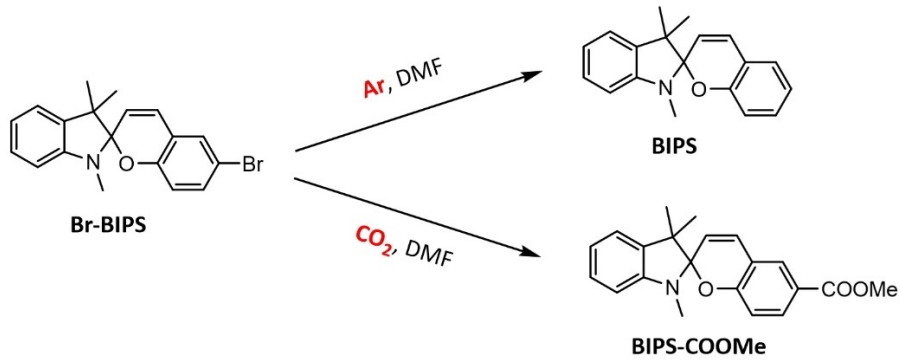

Working electrode (WE)	E_{ap} (V)	Ar sat. atmosphere	CO_2 sat. atmosphere	
		BIPS yield (%)	BIPS-COOMe yield (%)	BIPS yield (%)
Glassy C	-2.35	56	16	36
Ag	-2.00	91	35	30

Figure 6. Representation of the different products obtained depending on the conditions of the electrolysis and the yield resulted in each case.

employed (31% and 54% yield if the recovered initial reagent is taken into account). From this data, we could not only verify the electrocarboxylation of **Br-BIPS** as shown in Scheme 2, but also conclude that the use of silver cathodes to conduct this process presents several advantages resulting from their electrocatalytic properties. First, the reductive cleavage of the C–Br bond of the starting material takes place at lower potentials, which makes the reaction less energy consuming and, more importantly, increases the lifetime of the resulting reactive carbanion. Second, this leads to both larger conversion of the initial starting product (up to 65%) and formation of the target electrocarboxylated compound, which is eventually obtained at moderate yields (about 50% taking into account the reactant consumption).

The electrochemical response of the formed product **BIPS-COOMe** was compared to those of the precursor **Br-BIPS** and the byproduct of the reductive electrolysis **BIPS**. As shown in Figure 7, the potential of the cathodic peak associated with the first electron transfer toward these compounds varies depending on the nature of the substituent at the benzopyran ring. This behavior is related to the electronic character of each of these groups. In the case of **Br-BIPS**, E_{pc} is about 249 mV less negative than **BIPS**; i.e., it shows a larger tendency to be reduced than **BIPS**. This means that the inductive electron withdrawing effect of the bromide substituent in **Br-BIPS** is more important than its mesomeric electron donating effect. The nature of the irreversible two-electron transfer reduction process of **BIPS** was investigated by conducting a controlled potential electrolysis of this product at −2.6 V vs. SCE under nitrogen atmosphere. This revealed the formation of hydrogenated byproducts by reduction of **BIPS** olefinic bonds, a finding that corroborates the need of carefully controlling the conditions applied during the reductive activation of **Br-BIPS** to product the reactive species **BIPS**$^-$: because of the small difference in potential of the first cathodic waves of **Br-BIPS** and **BIPS**, the use of too long electrolysis times or large E_{ap} values could lead to the formation of undesired hydrogenated byproducts of **Br-BIPS**. Finally, in the case of **BIPS-COOMe**, a further decrement in the absolute value of E_{pc} was registered (447 mV relative to **BIPS**), which can be attributed to the presence of the strong electron withdrawing ester substituent.

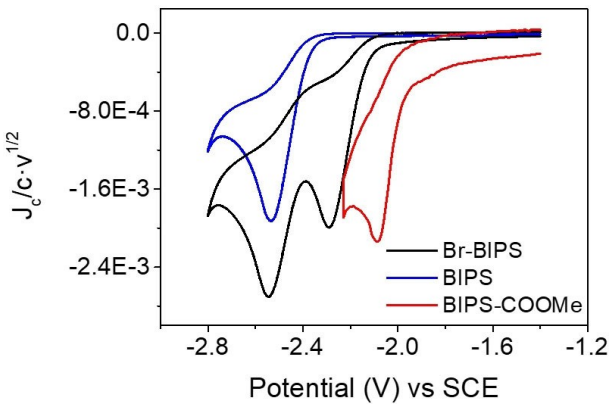

Figure 7. Normalized CV representing the electrochemical reduction response of Br-BIPS, BIPS and BIPS-COOMe in DMF/0.1 M $TBAPF_6$ with WE_c. Please note that the second reduction peak observed for Br-BIPS corresponds to the reduction of the BIPS molecules formed after the first electron transfer reaction.

Photochromism of electrochemically synthesized molecular switches

The photochromic response of spiropyrans **BIPS**, **BIPS-COOMe** and **Br-BIPS** (0.5 mM) was explored in dimethyl sulfoxide (DMSO) at room temperature (Figure 8). As expected, the most thermodynamically stable isomer, for all the three compounds in the dark, was found to be the spirocyclic form **SP**, with a maximum absorption peak located at ~295 nm for all three samples and a molar absorption coefficient of $\varepsilon = 3310–$

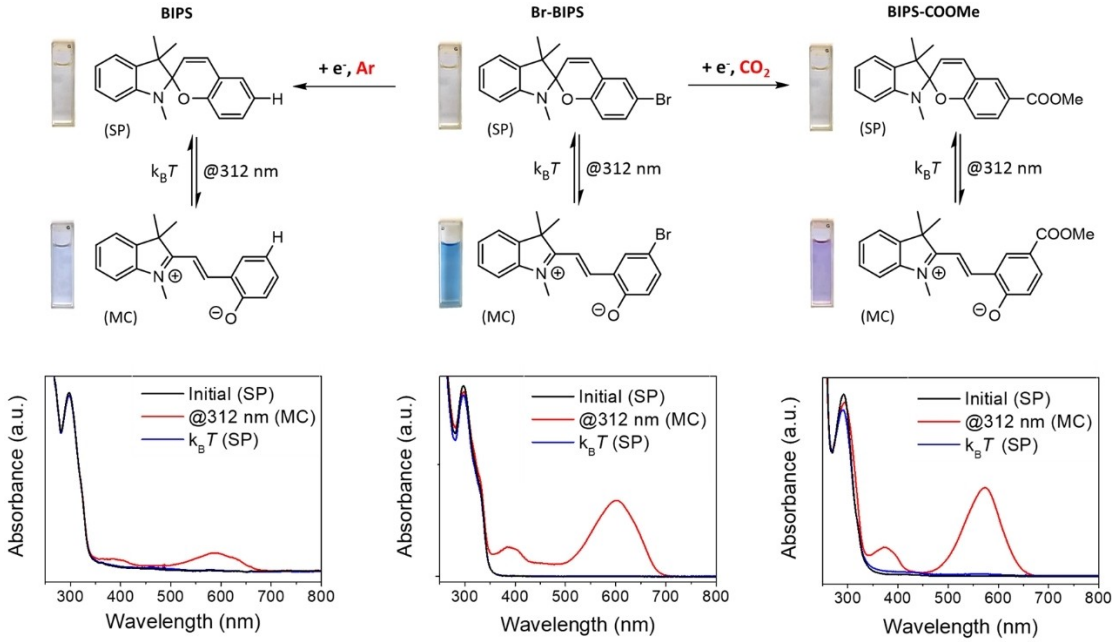

Figure 8. Absorbance UV-vis spectra of a 0.5 mM in DMSO of the reactant **Br-BIPS** showing the photochromic response of the molecular switch and the photochromic response of the switches, **BIPS** and **Br-BIPS** 0.5 mM in DMSO, electrochemically obtained. The switching between the closed (**SP**) to the colored (**MC**) forms for the different molecular switches were achieved when irradiating at @312 nm. The back conversion to the **SP** form was totally reached spontaneously over time in the dark.

4586 $M^{-1}cm^{-1}$ (Table 1). After irradiation of the samples with UV light (312 nm), the closed **SP** isomer opens via C_{spiro}—O bond breakage leading to the formation of the open **MC** form. This results in coloration of the solution as shown in Figure 8, because the merocyanine isomer formed presents a new absorption band at 573–601 nm.[51] An hypsochromic shift in absorption was noticeable when comparing the λ_{max} of the **MC** form depending on the nature of the substituting group at the 6 position in the benzopyran moiety; i.e., for **BIPS-COOMe** relative to **BIPS** and **Br-BIPS**.

It was found that, after irradiation at 312 nm for 2 minutes, all three molecular switches reached their photostationary state (PSS). The photochromic behavior of the switches was totally reversible since the initial **SP** form was recovered when the solution was let in the dark over time due to thermal back isomerization, obtaining a 100% yield back conversion. Some differences were found in the back conversion rates from **MC** to **SP**. This fact is directly related to the stability of the **MC** form, which in the case of **BIPS** was lower compared than for **Br-BIPS** and **BIPS-COOMe**. The presence of the electron-withdrawing bromo and ester substituents at the *para* position of the phenolate group of the **MC** form account for this result, as they aid stabilizing the negative charge of this group. Actually, this explains why, in the case of **Br-BIPS** and **BIPS-COOMe**, greater conversions to **MC** could be obtained compared to **BIPS** (Table 1 and Figure S5). Thus, it can be determined that it is possible to electrochemically access a variety of molecular switches with photochromic properties.

Table 1. Photochemical and electrochemical data extracted from the absorbance UV-Vis spectra and CV of **Br-BIPS**, **BIPS**, **BIPS-COOMe** upon irradiation and acidic conditions.

Name	State	λ_{max}, nm (ε, $M^{-1}cm^{-1}$)	k (s^{-1}) (MC→SP)	$E_{p,c}$ (V)
Br-BIPS	SP	297, shoulder (6293)	0.01986	−2.23
	SPH^+	297		
	MC	601		
	MCH^+	428		
BIPS	SP	296 (8274)	0.0362	−2.53
	SPH^+	295		
	MC	585		
	MCH^+	418		
BIPS-COOMe	SP	292 (8719)	0.0186	−2.08
	SPH^+	286		
	MC	573		
	MCH^+	*409*		

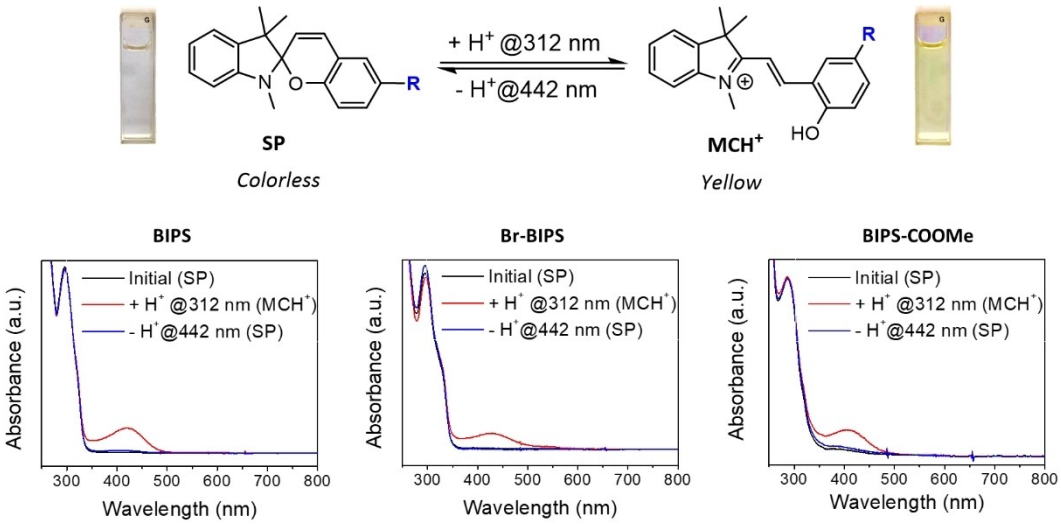

Figure 9. Switching properties of Br-BIPS, BIPS and BIPS-COOMe in slightly acidic DMSO when irradiating at 312 nm (c = 0.5 mM). Formation of the yellow-colored, protonated MCH^+ form is observed by means of absorption spectroscopy for all three compounds, which can revert back to the unprotonated SP state upon irradiation at 442 nm.

Photo-halochromism of electrochemically synthesized molecular switches

In addition, it was also determined the responsiveness of the spiropyran photoswitches developed in this work upon changes in pH, i.e., their photo-halochromism. For this, we consider the use of slightly acid media, where the **SP** form of spiropyrans is known to remain unprotonated because of its low pKa while the more basic **MC** isomer must become protonated into $\mathbf{MCH^+}$.[52,53] As seen in Figure 9, this was proven by irradiating with UV light acidic DMSO solutions of **Br-BIPS**, **BIPS** and **BIPS-COOMe**: instead of observing the blue coloration arising from **MC** formation with $\lambda_{abs,\ max} > 550$ nm, we obtained yellow solutions with new absorption bands with a maximum wavelength located around 409–428 nm, which are generally ascribed to the protonated merocyanine form **MCH** (Table 1). This process was found to be totally reversible, as the $\mathbf{MCH^+}$ form of **Br-BIPS**, **BIPS** and **BIPS-COOMe** could be fully converted to the initial, non-protonated spiropyran state when irradiating at 442 nm.

Conclusion

The electrochemical reduction mechanism of **Br-BIPS** has been disclosed under nitrogen and CO_2 atmospheres using cyclic voltammetry and control potential electrolysis under nitrogen and carbon dioxide atmospheres using carbon and silver cathodes. This study proves that the electrochemical reduction follows an ECE mechanism involving a C–Br reaction cleavage that takes place after the first electron transfer. Based on these data, compound **Br-BIPS** has been used for activating, valorizing and capturing CO_2, since the electrogenerated **BIPS** anion reacts with CO_2 though a nucleophilic attack. The use of silver cathodes allowed achieving moderate yields and efficiencies of electrocarboylated products under mild conditions thanks to its electrocatalytic properties. Finally, the *green* efficient electrochemical route described in the current work would open a new sustainable strategy for designing and building "smart" surfaces with switchable physical properties by s using CO_2 as a C1-organic building block.

Acknowledgements

The authors thank the Ministerio de Ciencia e Innovación of Spain for financial support though the project PID2019-106171RB–I00. S.M. acknowledges the Autonomous University of Barcelona for her predoctoral PIF grant.

Conflict of Interest

The authors declare no conflict of interest.

Data Availability Statement

The data that support the findings of this study are available from the corresponding author upon reasonable request.

Keywords: Carbon-Bromide cleavage · Carbon dioxide · Electrocarboxylation · CO_2 capture · spiropyran switches

[1] B. L. Feringa, *Molecular Switches*, WILEY-VCH, Weinheim, Germany, **2001**.
[2] G. Berkovic, V. Krongauz, V. Weiss, *Chem. Rev.* **2000**, *100*, 1741–1754.
[3] R. Tong, H. D. Hemmati, R. Langer, D. S. Kohane, *J. Am. Chem. Soc.* **2012**, *134*, 8848–8855.
[4] N. Tamai, H. Miyasaka, *Chem. Rev.* **2000**, *100*, 1875–1890.
[5] L. Kortekaas, W. R. Browne, *Chem. Soc. Rev.* **2019**, *48*, 3406–3424.

[6] N. Voloshin, E. Voloshina, M. Chernov'yants, A. Chernyshev, *Russ. J. Gen. Chem.* **2002**, *72*, 1468–1472.
[7] A. A. García, S. Cherian, J. Park, D. Gust, F. Jahnke, R. Rosario, *J. Phys. Chem. A* **2000**, *104*, 6103–6107.
[8] F. M. Raymo, S. Giordani, *J. Am. Chem. Soc.* **2001**, *123*, 4651–4652.
[9] C. Berton, D. M. Busiello, S. Zamuner, E. Solari, R. Scopelliti, F. Fadaei-Tirani, K. Severin, C. Pezzato, *Chem. Sci.* **2020**, *11*, 8457–8468.
[10] N. A. Murugan, S. Chakrabarti, H. Ågren, *J. Phys. Chem. B* **2011**, *115*, 4025–4032.
[11] L. Zhu, W. Wu, M.-Q. Zhu, J. J. Han, J. K. Hurst, A. D. Q. Li, *J. Am. Chem. Soc.* **2007**, *129*, 3524–3526.
[12] H. Görner, *Phys. Chem. Chem. Phys.* **2001**, *3*, 416–423.
[13] N. W. Tyer, R. S. Becker, *J. Am. Chem. Soc.* **1970**, *92*, 1289–1294.
[14] A. Goulet-Hanssens, F. Eisenreich, S. Hecht, *Adv. Mater.* **2020**, *32*, 1905966.
[15] M.-M. Russew, S. Hecht, *Adv. Mater.* **2010**, *22*, 3348–3360.
[16] S. Santiago, P. Giménez-Gómez, X. Muñoz-Berbel, J. Hernando, G. Guirado, *ACS Appl. Mater. Interfaces* **2021**, *13*, 26461–26471.
[17] S. Wu, J. Fan, W. Wang, D. Yu, *Colloids Surf. A* **2022**, *632*, 127760.
[18] R. Feringa, H. S. Siebe, W. J. N. Klement, J. D. Steen, W. R. Browne, *Mater. Adv.* **2022**, *3*, 282.
[19] P. Hong, L. Wang, L. Bai, Z. Liu, Y. Liu, J. Yang, A. Ying, *Dyes Pigm.* **2022**, *197*, 109902.
[20] S. Tian, J. Zhang, Q. Zhou, L. Shi, W. Wang, D. Wang, *Polymers (Basel).* **2021**, *13*, 2496.
[21] M.-Q. Zhu, L. Zhu, J. J. Han, W. Wu, J. K. Hurst, A. D. Q. Li, *J. Am. Chem. Soc.* **2006**, *128*, 4303–4309.
[22] H. Zhang, Z. Chen, Y. He, S. Yang, J. Wei, *ACS Appl. Mater. Interfaces* **2021**, *4*, 4340–4345.
[23] R. Tong, H. D. Hemmati, R. Langer, D. S. Kohane, *J. Am. Chem. Soc.* **2012**, *134*, 8848–8855.
[24] K. Tomizaki, H. Mihara, *Mol. BioSyst.* **2006**, *2*, 580.
[25] T. Sakata, Y. Yan, G. Marriott, *Proc. Nat. Acad. Sci.* **2005**, *102*, 4759–4764.
[26] N. Wagner, P. Theato, *Polymer* **2014**, *55*, 3436–3453.
[27] T. Garling, Y. Tong, T. A. Darwish, M. Wolf, R. K. Campen, *J. Phys. Condens. Matter* **2017**, *29*, 414002.
[28] J. Opel, L.-C. Rosenbaum, J. Brunner, A. Staiger, R. Zimmermanns, M. Kellermeier, T. Gaich, H. Cölfen, J.-M. García-Ruiz, *J. Mater. Chem. B* **2020**, *8*, 4831–4835.
[29] A. K. Bohaty, M. R. Newton, I. Zharov, *J. Porous Mater.* **2010**, *17*, 465–473.
[30] R. da Costa Duarte, F. da Silveira Santos, B. B. de Araújo, R. Cercena, D. Brondani, E. Zapp, P. F. B. Gonçalves, F. S. Rodembusch, A. G. Dal-Bó, *Chemosensors* **2020**, *8*, 31.
[31] M. Natali, C. Aakeröy, J. Desper, S. Giordani, *Dalton Trans.* **2010**, *39*, 8269.
[32] J. G. Pargaonkar, S. K. Patil, S. N. Vajekar, *Synth. Commun.* **2018**, *48*, 208–215.
[33] Y. Liu, J. Cornella, R. Martin, *J. Am. Chem. Soc.* **2014**, *136*, 11212–11215.
[34] T. E. Hurst, J. A. Deichert, L. Kapeniak, R. Lee, J. Harris, P. G. Jessop, V. Snieckus, *Org. Lett.* **2019**, *21*, 3882–3885.
[35] K. Kobayashi, Y. Kondo, *Org. Lett.* **2009**, *11*, 2035–2037.
[36] B. T. Sargent, E. J. Alexanian, *J. Am. Chem. Soc.* **2016**, *138*, 7520–7523.
[37] S. Mena, C. Louault, V. Mesa, I. Gallardo, G. Guirado, *ChemElectroChem* **2021**, *8*, 2649–2661.
[38] S. Mena, S. Santiago, I. Gallardo, G. Guirado, *Chemosphere* **2020**, *245*, 125557.
[39] S. Mena, G. Guirado, *C* **2020**, *6*, 34.
[40] S. Mena, J. Bernad, G. Guirado, *Catalysts* **2021**, *11*, 880.
[41] S. Mena, I. Gallardo, G. Guirado, *Catalysts* **2019**, *9*, 413.
[42] S. Mena, J. Sanchez, G. Guirado, *RSC Adv.* **2019**, *9*, 15115–15123.
[43] A. A. Isse, C. Durante, A. Gennaro, *Electrochem. Commun.* **2011**, *13*, 810–813.
[44] Z. Chami, M. Gareil, J. Pinson, J. M. Saveant, A. Thiebault, *J. Org. Chem.* **1991**, *56*, 586–595.
[45] C. Durante, A. A. Isse, F. Todesco, A. Gennaro, *J. Electrochem. Soc.* **2013**, *160*, G3073–G3079.
[46] C. Durante, A. A. Isse, G. Sandonà, A. Gennaro, *Appl. Catal. B* **2009**, *88*, 479–489.
[47] S. Arnaboldi, A. Bonetti, E. Giussani, P. R. Mussini, T. Benincori, S. Rizzo, A. A. Isse, A. Gennaro, *Electrochem. Commun.* **2014**, *38*, 100–103.
[48] S. Mena, J. Sanchez, G. Guirado, *RSC Adv.* **2019**, *9*, 15115–15123.
[49] I. Gallardo, G. Guirado, J. Marquet, *J. Electroanal. Chem.* **2000**, *488*, 64–72.
[50] J. Massaad, J. C. Micheau, C. Coudret, C. L. Serpentini, G. Guirado, *Chem. Eur. J.* **2013**, *19*, 12435–12445.
[51] S.-R. Keum, R. Se-Jung, K. Sang-Eun, L. Sung-Hoon, C. Chul-Hee, K. Sung-Hoon, K. Kwang-Nak, *Bull. Korean Chem. Soc.* **2006**, *27*, 187–188.
[52] L. Kortekaas, J. Chen, D. Jacquemin, W. R. Browne, *J. Phys. Chem. B* **2018**, *122*, 6423–6430.
[53] L. Wimberger, S. K. K. Prasad, M. D. Peeks, J. Andréasson, T. W. Schmidt, J. E. Beves, J. Am, *Chem. Soc. Rev.* **2021**, *143*, 49, 20758–20768.

Manuscript received: November 19, 2021
Revised manuscript received: December 24, 2021
Accepted manuscript online: January 10, 2022